Radiative Regimes in Gamma-Ray Bursts and Afterglows

A. Panaitescu & P. Mészáros
Department of Astronomy & Astrophysics,
Pennsylvania State University, University Park, PA 16802

ABSTRACT

We present numerical simulations of Gamma-Ray Bursts arising from external shocks in the impulsive and wind models, including a weak or a strong coupling between electrons and protons plus magnetic fields, and analyze the burst features in each scenario. The dynamics of the ejecta and external medium are followed into the late stages of deceleration, in order to study the hydrodynamics of the remnant and the temporal and spectral evolution of the afterglow. A brief comparison with the optical and radio afterglows of GRB 970228 and GRB 970508 is made.

Subject headings: gamma-rays: bursts - methods: numerical - radiation mechanisms: non-thermal

1. Introduction

Gamma-Ray Bursts (GRBs) are thought to be due to internal or external shocks in relativistic fireball outflows following a catastrophic compact binary merger or collapse. This view has received considerable support from recent observations of GRB afterglows in X-ray, optical and radio, extending in some cases over many months (e.g. Proceedings of the Fourth Huntsville GRB Symposium – Meegan, Preece & Koshut 1998). While the γ-ray emission of some bursts, particularly those with very many peaks, probably arises from internal shocks (Rees & Mészáros 1994, Sari & Piran, 1997), these should be followed in most cases by external shocks. The simplest afterglow model is provided by the time evolution of the decaying external shock (Mészáros & Rees 1997), and can explain the major features of observed afterglows (Wijers, Rees & Mészáros 1997, Tavani 1997, Vietri 1997, Waxman 1997a, Reichart 1997). In this paper, we simulate GRB afterglows in the framework of the external shock model (Mészáros & Rees 1993), whose γ-ray light curves are either fairly smooth or have a low ($\lesssim 10$) number of pulses (Panaitescu & Mészáros , 1998a). Our purpose is to investigate the properties of bursts and afterglows under different physical conditions which impact the dynamic regime of expansion of the remnant as well as the burst and afterglow spectrum.

The details of the hydrodynamic code and of the energy release and transfer model used here (including assumptions and approximations) are presented in Panaitescu & Mészáros (1998a). Here we mention only the most important assumptions and the new features included :

1. The electrons are initially accelerated by one of the two shocks ("reverse" and "forward") that sweep up the relativistic ejecta or the external medium, respectively. The distribution of electrons is a power-law of index $p = 2.5$, from a minimum Lorentz factor γ_m to a maximum γ_M. The γ_m is derived from the total energy of electrons, assumed to be a fraction ε_{el} of the internal energy of the shocked fluid: $\gamma_m = 610\,\varepsilon_{el}\Gamma$, where Γ is the flow Lorentz factor. γ_M is upper bounded by the condition that electrons with this Lorentz factor can be accelerated on timescale shorter than their cooling timescale.

2. The electrons lose energy through synchrotron emission in the presence of a turbulent magnetic field, and through inverse Compton of the self-produced synchrotron photons. The magnetic field

intensity B' is parameterized by the fraction ε_{mag} of the internal energy stored in the magnetic field: $B'^2/8\pi = \varepsilon_{mag} n'_e m_p c^2 \Gamma$, where $n'_e = 4\Gamma n_{ext}$ is the co-moving density of the shocked fluid, n_{ext} being the number density of the decelerating medium. At equipartition between electrons, protons and the magnetic field, $\varepsilon_{el} = \varepsilon_{mag} = 1/3$.

3. In the *weak coupling model* the energy transfer from protons and magnetic field to electrons takes place on a hydrodynamic (deceleration) timescale t_{dec}. In the *strong coupling model* electrons are assumed to be re-accelerated on a timescale much shorter than t_{dec} (e.g. by repeated scatterings on magnetic field inhomogeneities, or other mechanisms). These are two extreme situations; in general such re-accelerations should occur on an intermediate timescale that must be treated as a new free parameter, due to the relatively poor present understanding of the microscopic processes that could be at work here.

4. Unlike in our previous paper, we use now the full shape of the synchrotron spectrum to calculate the emission from the two shocks. However, for higher computational efficiency, we maintain the previous "monochromatic approximation" when calculating the inverse Compton (IC) spectrum: before up-scattering, the spectrum of the synchrotron radiation from each shock is approximated as monochromatic, at an intensity-weighted frequency. Furthermore, the IC spectrum from the electrons in each infinitesimal volume element is approximated as monochromatic, at the peak frequency for a given electron Lorentz factor and energy of incident synchrotron photon.

5. Self-absorption of low energy (radio and optical) photons and the destruction of high energy photons ($\gtrsim 1\,\mathrm{GeV}$) through pair creation during propagation from source to observer are not taken into account. We consider cosmological effects, assuming that the source is located at redshift $z = 1$ and that $H_0 = 75\,\mathrm{km\,s^{-1}Mpc^{-1}}$ and $\Omega = 1$.

The interaction between the expanding shell and the external matter is simulated using a 1D hydrodynamical code suitable for relativistic flows involving shocks. The temporal features (i.e. bolometric and band light-curves) and spectral features (a set of instantaneous spectra and the averaged spectrum) of the burst are calculated by integration over lab-frame time, volume of the shocked fluid and electron distribution. As pointed out by Waxman (1997b), most of the radiation received by the observer at given time T comes from a ring whose width is relatively small compared to the size $\sim \Gamma(T)\, cT$ of the visible disk, where $\Gamma(T)$ is the Lorentz factor of the fluid moving exactly toward the observer. We found that the shape of the source, as seen by the observer in a given band, changes from an almost uniformly bright disk to a ring whose width (defined as the on-sky projected size of the zone that radiates 50% of the energy received at detector) is between 6% and 21% of the radius of the source's projection on the sky (Panaitescu & Mészáros 1998b). The fluid seen in this ring is shocked earlier than the fluid moving with $\Gamma(T)$ on the line of sight toward the center of explosion, and thus they have different physical parameters (γ_m, B', Γ). This is taken into account in the analytic calculations presented in §3.

2. Radiative Dynamics and Gamma-Ray Emission

We investigate here the effect of a continuous energy transfer between protons plus magnetic fields and the radiating electrons on the hydrodynamics of the interaction, the burst light-curve, its spectral hardness and softening. For the fireball we first consider the impulsive model and after that we use the wind model to obtain a wider and less dense fireball when deceleration becomes important (t_{dec}) and thus a more relativistic reverse shock.

The peak of the synchrotron emission from the forward shock, which dominates the overall emission of

the burst and the afterglow, is at an observer energy

$$h\nu_p = 1.4\times10^{-8}\,(1+z)^{-1}\gamma_m^2 B'\Gamma\ \mathrm{eV} = 10^{-3}\,[(1+z)/2]^{-1}\varepsilon_{el}^2(\varepsilon_{mag}n_0)^{1/2}\Gamma^4\ \mathrm{eV}\ , \qquad (1)$$

where we used the synchrotron critical frequency corresponding to γ_m, averaged over the pitch angle, and n_0 is the external medium particle density in cm^{-3}. For a fireball initial Lorentz factor Γ_0, the average flow Lorentz factor during the main burst is $\Gamma_\gamma \sim (1/2)\Gamma_0$. In all simulations discussed below, the initial Lorentz factor is $\Gamma_0 = 500$ and the energy release parameters ε_{el} and ε_{mag} have been chosen at the maximum value (i.e. equipartition). Then equation (1) gives $h\nu_p \sim 250\,\mathrm{keV}$. For this Γ_0 values of these parameters too much below equipartition would lead to spectral peaks below the first BATSE channel (lower edge at $\sim 25\,\mathrm{keV}$). If the electron acceleration timescale is taken to be its gyration period, then $\gamma_M \sim 5\times10^7\,(B/1\,\mathrm{G})^{-1/2} \sim 8\times10^7\,(\varepsilon_{mag}n_0)^{-1/4}\Gamma^{-1/2}$. Thus, during the GRB, $\gamma_M/\gamma_m \sim 30\,\varepsilon_{el}^{-1}(\varepsilon_{mag}n_0)^{-1/4}(\Gamma_0/500)^{-3/2}$, implying $\gamma_M/\gamma_m \sim 120$ for $\Gamma_0 = 500$ and equipartition.

Figure 1 shows the average burst spectrum for an impulsive fireball with weak coupling in the shocked fluid. It has six components: one synchrotron and two inverse Compton from each shock. Behind the reverse shock, inverse Compton scatterings of locally produced photons take place in the Thomson regime; behind the forward shock these scatterings occur in the extreme Klein-Nishina regime and substantial up-scattered radiation is emitted only after electrons have cooled; mixed scatterings take place in a mild Klein-Nishina regime. The steep cut-off that can be seen above the synchrotron FS peak in Figure 1 (and also in Figure 2) is due to the fact that very energetic electrons ($\gamma_M/\gamma_m > 10$) have very short cooling timescales and tracking their evolution accurately, by choosing a computational timestep smaller than this short synchrotron cooling timescale, would lead to very long runs. Therefore the cut-off seen above ~ 10 MeV arises from choosing a low value of the ratio γ_M/γ_m and should be regarded as a deficiency of purely computational origin, and not as a deficiency of the fireball model.

In the weak coupling model, electrons are accelerated and exchange energy with protons and magnetic fields only at the shock, but not anywhere else in the flow. Such electrons cool very fast in a burst that has $h\nu_p$ above 50 keV. Thus, on timescales shorter than t_{dec}, a good fraction of the available internal energy of the shocked fluid remains locked up in protons. This fraction is larger than 1/2 because the fluid is continuously decelerated and more and more internal energy is produced. Nevertheless the evolution of the shocked fluid after electron cooling is not totally adiabatic, as the internal energy is used to drive forward the blast wave that sweeps up the external medium and to accelerate new electrons capable of radiating away the internal energy. On the other hand, if electrons are re-accelerated behind the forward shock (strong coupling model), then the internal energy is depleted very fast and the shocked structure stays in a radiative regime for longer times, until the electron themselves become adiabatic. If the re-acceleration timescale is much longer than the cooling timescale (as is the case in the weak coupling scenario), the electron spectrum will have an index $p/2$, due to the cooling and the continuous electron injection at the shock, while if the re-acceleration takes place on a timescale shorter than the cooling timescale (weak coupling model), the spectral index will be $(1/2)(p-1)$. Therefore, one expects the strong coupling model burst to show a photon spectrum harder than for the weak coupling model. The self-inverse Compton scatterings are in the extreme Klein-Nishina regime for a longer time than in the weak coupling model, making the inverse Compton scattering less efficient for electron cooling (see Figure 2).

In the *impulsive model*, the co-moving frame density of the fireball when deceleration becomes important (at time $t \lesssim t_{dec}$) is $\sim \Gamma_0^2$ times larger than that of the external medium. The reverse shock is quasi-newtonian ($\Gamma_R \simeq 1.1$) in the frame of the yet unshocked fireball, while the forward shock moves in the lab-frame with $\Gamma_F \gtrsim 300$. Such a reverse shock is inefficient in converting the ejecta's kinetic energy

into heat (the ratio of the internal and rest-mass energy density behind the shock is $\Gamma_R - 1$). A more relativistic reverse shock can be obtained if the fireball is less dense, which, for the same mass, requires a larger thickness. This can be achieved if the fireball results from an energy release that lasted more than few seconds (*wind model*). For a wind of duration $t_{wind} = 33$ s, the lab-frame fireball thickness is 10^{12} cm, ~ 10 times larger than in the impulsive scenario. In this case $\Gamma_R \simeq 1.5$ and $\Gamma_F \simeq 180$. A more relativistic reverse shock radiates more efficiently, while a less relativistic forward shock leads to a softer and weaker GRB, as shown in Figure 2 (long dashed curve) by the relative intensity and position of the peaks of the synchrotron emission from the two shocks.

In Figure 3 we compare the light-curves and spectral evolution of the bursts obtained in three models: impulsive with weak or strong coupling, and wind with strong coupling. The left graph legend indicates that the reverse shock contributes more to the observed burst if there is a strong coupling, which is due to the fact that the continuously generated internal energy behind the reverse shock is radiated, rather than being stored in protons and used to push the forward shock (and thus released in the end by the forward shock). The same legend gives the temporal asymmetry defined as $\int_{T_p}^{\infty} F_{23}(t)dT / \int_0^{T_p} F_{23}(T)dT$, where F_{23} is the flux in the second and third BATSE channels (50 keV – 1 MeV) and T_p is the peak time. The temporal asymmetry observed in real bursts is between 1.4 and 2.0 (Mitrofanov et al. 1996), smaller than that of the bursts arising from an impulsive release of the ejecta. The $T^{-\alpha}$ decay of the burst is steepest in the wind model (see legend of left graph in Figure 3). The burst γ-ray efficiency (ratio of fluence in the BATSE four channels, 25 keV – 1 MeV, and the bolometric fluence) is the lowest in the same model, $\sim 30\%$ compared to the 50% efficiency reached in the impulsive models. The right graph of Figure 3 shows that for the same parameters $(\Gamma_0, n_0; \varepsilon_{mag}, \varepsilon_{el})$, the wind model produces a soft burst with the slowest softening rate, while the impulsive model with strong coupling gives the hardest burst. One would expect these features to be present not only in single-hump bursts but also in the individual pulses of those bursts with a modest time variability.

The external shock model is able to explain well established features of GRBs, such as (1) the brightness–spectral hardness correlation, (2) the spectral hardening before an intensity pulse superposed on a continuous spectral softening, and (3) pulses peak earlier and last shorter at higher energies, as shown in Panaitescu & Mészáros (1998a). The synchrotron thin model considered here is not able to account for values of the low energy spectral slope larger than 1/3 (4/3 for νF_ν) (Crider et al. 1997, Preece et al. 1998, Strohmayer et al. 1998). As mentioned in the previous section, the external shock model is not able to explain without the use of extra assumptions (e.g. a rapidly varying magnetic field combined with a highly anisotropic radiation emission in the co-moving frame) the large number of pulses observed in many GRBs. We have considered here GRB light-curves and spectra in the framework of this model only for the purpose of comparing the effects of an extended and impulsive energy release and those of a strong and weak coupling in the fireball. Even if the burst itself arises from internal shocks (Rees & Mészáros 1994), one expects the external shock to be at work when the fireball runs into the surrounding medium.

3. Afterglows

The spectral evolution of the afterglow is mainly determined by that of the bulk Lorentz factor of the shocked fluid and we will assume all other parameters (such as ε_{mag} and ε_{el}) to be constant. We consider the impulsive model with weak or strong coupling in the remnant. In the absence of a strong coupling, electrons cool fast and most of the burst emission comes from the leading edge of the shocked external matter (immediately behind the blast wave). If a strong coupling is present, then all the fluid heated by the

two shocks radiates efficiently.

The general expected behavior of Γ during the relativistic phase is $\propto t^{-n}$, where t is the lab-frame time, $n = 3$ if the remnant is radiative, and $n = 3/2$ if it is adiabatic (Blandford & McKee 1976). Numerically we found that the remnant Lorentz factor can be approximated by

$$\Gamma \simeq \Gamma_\gamma (t/t_{dec})^{-n} \ , \tag{2}$$

for $t > t_{dec}$ and before the beginning of the non-relativistic regime, where

$$t_{dec} = 1.4 \times 10^6 \, (E_{52}/n_0)^{1/3} (\Gamma_0/500)^{-2/3} \, \mathrm{s} \ . \tag{3}$$

t_{dec} is the time when the mass of the swept up external fluid is a fraction Γ_0^{-1} of the ejecta's mass, representing the deceleration onset time (Rees & Mészáros 1992). In equation (3) $E = 10^{52} E_{52} \omega_{jet}$ ergs is the total amount of energy released in the ejecta, where ω_{jet} is the solid angle of the ejecta. In a radiative remnant the electrons must be themselves radiative: $t_{sy} < t_{ad}$. Here t_{sy} is the lab-frame electron cooling timescale, which is practically determined only by synchrotron cooling:

$$t_{sy}(\gamma_m) = 8.4 \times 10^6 \, (\varepsilon_{el} \varepsilon_{mag} n_0)^{-1} \Gamma^{-2} \, \mathrm{s} \ , \tag{4}$$

and t_{ad} is the adiabatic cooling timescale. The shell of shocked external matter is compressed between the contact discontinuity and the forward shock, the increase in the shell thickness in time being rather due to the continuous accumulation of external matter than to a radial expansion of the shell. Thus, to a good approximation, $t_{ad} = (2^{3/2} - 1)\, t = 1.83\, t$. Using equations (2) and (4), it results that for $n = 3$ electrons become adiabatic when Γ drops below

$$\Gamma_{r \to a} = 2.5 \, (9 \, \varepsilon_{el} \varepsilon_{mag})^{-3/5} n_0^{-2/5} E_{52}^{-1/5} (\Gamma_0/500)^{1/5} \ . \tag{5}$$

Therefore, at equipartition, electrons are radiative as long as the radiative remnant is relativistic.

The evolution of Lorentz factor of the fluid moving on the line of sight toward the center (lsc) of explosion (i.e. pointing exactly toward the observer) can be calculated analytically from $dT = (1+z)\, dt/(4\,\Gamma^2)$, where T is the arrival time of the photons emitted at shock and on the lsc. The result can be cast into the simple form

$$\Gamma_{lsc}(T) = C_n \, \Gamma_\gamma (T/T_\gamma)^{-n/(2n+1)} \ , \tag{6}$$

where $T_\gamma \equiv 2\,(1+z)\, t_{dec} \Gamma_\gamma^{-2} = 92 \, [(1+z)/2] (E_{52}/n_0)^{1/3} \Gamma_0^{-8/3}$ s is a good approximation[1]of the γ-ray burst duration. For a radiative remnant ($n = 3$), one can show that $C_3 = 0.18$. If there is a strong coupling, the remnant and the electrons become adiabatic simultaneously, at a time $T_{r \to a}$ that can be calculated using equations (5) and (6). After that, the evolution of Γ_{lsc} is given by equation (6) with $n = 3/2$ and a coefficient

$$C_{3/2} = 0.13 \, (9 \, \varepsilon_{el} \varepsilon_{mag})^{-3/40} n_0^{-1/20} E_{52}^{-1/40} (\Gamma_0/500)^{-1/10} \tag{7}$$

that has a very weak dependence on the burst parameters. For the weak coupling remnant we found numerically that (if the energy release parameters are not much below equipartition) the quasi-adiabatic regime starts early in the afterglow, at times when the spectrum peaks in the soft UV. An analytic

[1]This definition was chosen to match the duration obtained numerically (see Figure 3, left graph) and is larger by a factor 16 than the usual result $T_\gamma \sim (1+z)\, t_{dec}/(2\,\Gamma_0^2)$, which does not take into account the angular spreading contribution to the burst duration, and the fact that $\Gamma \lesssim \Gamma_0/2$ during most of the γ-ray emission

calculation of the time when the weak coupling remnant becomes adiabatic is too inaccurate and we shall further use for the coefficient in equation (6) a value inferred from numerical results: $C_{3/2} = 0.32$. Thus, for the adiabatic remnant with weak coupling

$$\Gamma_{lsc,wc} = 6.1\ (E_{52}/n_0)^{1/8}[(1+z)/2]^{3/8}T_d^{-3/8}\ , \tag{8}$$

where T_d is the observer time measured in days. Note that if $C_{3/2}$ does not depend too strong on the burst parameters (as suggested by the eq. [7] for the strong coupling case), then $\Gamma_{lsc,wc}$ has a weak dependence on the model parameters. If the evolution of Γ is the most important factor in determining the afterglow's features, then external shock GRBs arising from fireballs with different Γ_0's, exhibiting thus very different timescales, should be followed by afterglows that have similar timescales.

The afterglow that follows the burst of Figure 1 (weak coupling) is shown in Figure 4. As the forward shock decelerates, the synchrotron emission from it shifts toward lower energies as $h\nu_p \propto T^{-1.4}$, consistent with the adiabatic regime of the remnant $\Gamma \propto t^{-1.5}$. At all times the intensity of the IC up-scattered emission is below that of the synchrotron one, which shows that inverse Compton is less efficient in electron cooling than synchrotron emission. 90% of the initial fireball energy is released during the weak-coupling afterglow shown in Figure 4. The wide-band distribution of the energy radiated is: 35% as γ-rays (above 100 keV), 35% as X-rays (1 keV – 100 keV), 21% in the UV (1 eV – 1 keV), 5% in optical (1 eV – 10 eV) and 5% in IR and radio (below 1 eV). For a strong coupling remnant, the distribution is 49%, 22%, 19%, 5% and 5%, respectively. Note that the strong coupling case leads to a higher γ-ray fluence at the expense of a lower X-ray fluence.

Equation (1) gives the peak of the synchrotron radiation assuming that the γ_m-electrons give almost all the burst radiation, which is correct only if electrons are not re-accelerated on a very short timescale. This equation may under-estimate the true value of $h\nu_p$ in the case of a continuous post-shock re-acceleration on a timescale shorter than the cooling timescale, when νF_ν is expected to have a positive slope $(1/2)(3-p)$ for $p < 3$. In this case, due the fact that photons received simultaneously by the observer were emitted at different lab-frame times, thus from shocked material with different γ_m, B' and Γ, the real peak of νF_ν is at a frequency higher than $\nu(\gamma_m)$, that cannot be accurately calculated analytically. For simplicity, we will proceed with the analytical derivations assuming that the synchrotron spectrum peak ν_p is determined only by γ_m, as given by equation (1).

An estimate of the time T_{ν_p} when the peak of νF_ν reaches a given observational frequency ν_p and of the source size at that time can be obtained using the geometry of the equal arrival time surface described by Panaitescu & Mészáros (1998b). From equation (1), the flow Lorentz factor of the fluid that gives most radiation at detector frequency ν_p is $\Gamma_{\nu_p} = (\nu_p/\nu_\gamma)^{1/4}\Gamma_\gamma$, where ν_γ is the synchrotron peak frequency during the γ-ray burst. Most of this fluid is off-set from the *lsc* and we shall denote by $f_\parallel$ the ratio between the projection onto the *lsc* of the radial coordinate (measured from the center of explosion) of the region that gives most of the radiation and the radial coordinate of the fluid on the *lsc*. This ratio must be determined from the geometry of the equal arrival time surface. The Lorentz factor of the fluid on the *lsc* and on the equal-T_{ν_p} surface is $\Gamma_{lsc} = f_\parallel^n\Gamma_{\nu_p} = f_\parallel^n(\nu_p/\nu_\gamma)^{1/4}\Gamma_\gamma$. Using equation (6), $T_{\nu_p} = (C_n^{1/n}f_\parallel^{-1})^{2n+1}(\nu_\gamma/\nu_p)^{(2n+1)/4n}T_\gamma$. For an adiabatic remnant ($n = 3/2$, $C_{3/2} = 0.32$, $f_\parallel = 0.82$)

$$T_{\nu_p} = 6.3\left(\frac{h\nu_\gamma}{100\,\mathrm{keV}}\right)^{2/3}\left(\frac{h\nu_p}{1\,\mathrm{eV}}\right)^{-2/3}T_{\gamma,2}\ \mathrm{hours}\ , \tag{9}$$

where $T_\gamma = 100\,T_{\gamma,2}$ s. For the afterglow shown in Figure 4, $h\nu_\gamma = 250$ keV. Equation (9) leads to $T_{1\,eV} = 11$ h, consistent with the afterglow spectral softening shown in Figure 4.

The size of the source at time T, as seen projected on a plane perpendicular to the lsc, is $R_\perp = f_\perp \Gamma_{lsc}[cT/(1+z)]$, where $f_\perp = 2^{3/2}(2n+1)[2(n+1)]^{-(n+1)/(2n+1)}$. Using (6) with Γ_γ expressed as a function of ν_γ with the aid of equation (1), one finds for an adiabatic remnant ($n = 3/2$, $f_\perp = 4.1$) that, at equipartition,

$$R_\perp = 2.7 \times 10^{16} \left(\frac{1+z}{2}\right)^{-3/4} n_0^{-1/8} \left(\frac{h\nu_\gamma}{100\,\mathrm{keV}}\right)^{1/4} T_{\gamma,2}^{3/8} T_d^{5/8}\ \mathrm{cm}\ . \tag{10}$$

Equation (10) relates the remnant size to characteristics of the main burst. Using equation (8), the same size can be written as:

$$R_\perp = 3.2 \times 10^{16}\,(E_{52}/n_0)^{1/8}[(1+z)/2]^{-5/8} T_d^{5/8}\ \mathrm{cm}\ . \tag{11}$$

For the afterglow shown in Figure 4, $R_\perp = 3.2 \times 10^{16}\, T_d^{5/8}$ cm, thus the apparent source radius evolves as $\phi = 1.8\ T_d^{5/8}\,\mu$as. The source appears to the observer as a disk that is brighter near the edge than near the center. The width of the outer ring that radiates 50% of the radiation is $\sim 0.19\,\phi$. Equations (9) and (10) can be used to test the fireball model, once the duration and peak frequency of the main burst are measured.

Figure 5 shows a comparison between the time histories of the two bursts that had afterglows below the X-ray domain (February 28 and May 08) and the numerical simulations in both strong and weak coupling models. There are several disagreements between the real afterglows and the simulated ones, e.g. the much lower fluence of the February 28 burst in the $0.1\,\mathrm{keV} - 2\,\mathrm{keV}$ band at $T < 1$ day, the absence of a rise in the numerical V magnitude and the larger numerical flux densities at 4.9 GHz. The relatively steep falls that can be seen at $T \gtrsim 1$ day are due to the computational constraint described in the previous section, regarding the very short cooling synchrotron cooling time of the electrons in the high energy part of the power-law distribution, i.e. those electrons which give the X-ray emission.

The optical and radio fluxes we obtained may be higher than what was observed for the afterglows of GRB 970228 and 090508 due to the large fireball energy used in the numerical simulation[2]. The dependence on the burst parameters of the flux received at a fixed frequency ν can be obtained analytically from the flux at the peak frequency $F_{\nu_p} = (\Gamma T)^2(\Gamma^3 I'_{\nu'_p})$ (Mészáros & Rees 1997), where $I'_{\nu'_p} \sim (n'_e/4\,\pi)(P'_{sy}/\nu'_p)\min\,(ct'_{sy}, \Delta')$ is the co-moving intensity at the peak of the synchrotron emission from the least energetic electrons (γ_m). Here n'_e, P'_{sy}, t'_{sy} and Δ' are the co-moving electron density, synchrotron power, cooling timescale and remnant thickness. These quantities can be easily calculated and put together to yield F_{ν_p} as a function of $\Gamma \propto \Gamma_{lsc}$, which is given by equation (8) for an adiabatic remnant with weak coupling. One finds that for $\nu < \nu_p$ $F_\nu = (\nu/\nu_p)^{1/3} F_{\nu_p} \propto \varepsilon_{mag}^{-2/3}\varepsilon_{el}^{-5/3} E^{1/3} T \nu^{1/3}$ if electrons are radiative, and $F_\nu \propto \varepsilon_{mag}^{1/3}\varepsilon_{el}^{-2/3} n_0^{1/2} E^{5/6} T^{1/2} \nu^{1/3}$ if electrons are adiabatic, assuming in both cases an adiabatic remnant. Note that in the latter case F_ν depends rather strongly on the burst energy. At frequencies $\nu > \nu_p$ the monochromatic flux is $F_\nu = (\nu/\nu_p)^{-p/2} F_{\nu_p} \propto \varepsilon_{mag}^{1/8}\varepsilon_{el}^{3/2} E^{9/8} T^{-11/8} \nu^{-5/4}$ if electrons are radiative, and $F_\nu = (\nu/\nu_p)^{-(p-1)/2} F_{\nu_p} \propto \varepsilon_{mag}^{7/8}\varepsilon_{el}^{3/2} n_0^{1/2} E^{11/8} T^{-9/8} \nu^{-3/4}$ if electrons are adiabatic, for $p = 2.5$. In both cases, F_ν has a strong dependence on ε_{el} and the available energy E. The previous relationships were derived assuming that all electrons are in the same radiative regime. In reality, high energy electrons can remain radiative for much longer times than those with γ_m, altering somewhat the power-law indices

[2]A value of $E \sim 10^{53}$ ergs is used for an isotropic fireball to simulate a burst with a peak flux in the BATSE window $\sim 10^{-6}$ ergs cm^{-2}s^{-1}, corresponding to a peak photon flux $\sim 1\,\gamma\,\mathrm{cm}^{-2}\mathrm{s}^{-1}$, given a smooth external shock light-curve (multi-peaked bursts can reach a higher peak flux with a lower energy budget). Shorter duration bursts, with higher peak fluxes and requiring less energy, can be simulated using larger Lorentz factors Γ_0, which would however require longer numerical runs.

derived above. For example, if γ_m-electrons become adiabatic at time T_m, electrons with $\gamma_e = 2\gamma_m$ become adiabatic when Γ has decreased by a factor $\sqrt{2}$, which occurs at time $T_e = (\sqrt{2})^{8/3} T_m = 2.5\, T_m$.

Over-estimations of the radio and optical fluxes may also arise from the fact that we assumed a spherically symmetric ejecta. So far we worked with an initial energy release of 10^{52} ergs/sr, which is consistent with the "traditional" release of 10^{51} ergs if the ejecta are collimated in a jet of solid angle 0.1 sr (half angular opening $\simeq 11^{\rm o}$). Thus the observer would see the edge of this jet when Γ drops below 5, corresponding to $T \gtrsim 2$ day in our example. The error made in the numerical simulation, which assumed spherical symmetry, increases with time as the jet opening angle becomes smaller and smaller than Γ^{-1}, the angular opening of the surface over which the emitted radiation was integrated. Thus fluxes are over-estimated by a factor ~ 1.2 (approximately 0.2 magnitudes) at $T = 2$ days and by a factor 2.2 (corresponding to 0.8 magnitudes) at $T = 10$ days.

Numerical over-estimations of the flux at radio frequencies are also due to the fact that we did not take into account the synchrotron self-absorption. It is easy to find out the time dependence of the self-absorption frequency ν_{ab}, but it is not a trivial exercise to calculate an accurate value of it. If the synchrotron self-absorption coefficient is used, one should take into account the relativistic expansion of the absorbing fluid during the propagation of a photon through it. Here, we shall use the equality of the self-absorbed intensity $(I'_{\nu'})_{abs} \sim 2\,\gamma_m m_e \nu'^2$ (m_e is the electron's mass) and the synchrotron intensity $(I'_{\nu'})_{p-law} \sim (\nu'/\nu'_p)^{1/3} I'_{\nu'_p}$ for a power-law distribution of electrons, at the unknown frequency ν'_{ab} (primed quantities are measured in the co-moving frame). In both kinds of calculations of ν_{ab}, the shape of the equal arrival time surface must be taken into account. In the method chosen here to calculate ν_{ab}, this is taken into account by using the Lorentz factor Γ of the fluid that dominates the flux received by the observer, which is related to Γ_{lsc} by $\Gamma = f_{\parallel}^{-n} \Gamma_{lsc}$. The end result is that for an adiabatic remnant with weak coupling $\nu_{ab} = 0.37\, \varepsilon_{mag}^{-2/5} \varepsilon_{el}^{-8/5} n_0^{3/10} E_{52}^{-1/10} [(z+1)/2]^{-13/10} T_d^{3/10}$ GHz if electrons are radiative, and $\nu_{ab} = 1.6\, \varepsilon_{mag}^{1/5} \varepsilon_{el}^{-1} n_0^{3/5} E_{52}^{1/5} [(z+1)/2]^{-1} T_d^0$ GHz if electrons are adiabatic. For the representative values used so far and at equipartition, one obtains $\nu_{ab} = 3.3\, T_d^{3/10}$ GHz for radiative electrons and $\nu_{ab} = 3.8\, T_d^0$ GHz for adiabatic electrons. Thus one expects the remnant to be optically thin at 8.46 GHz, $\tau_{4.86\ {\rm GHz}} \sim 1$, and optically thick at 1.43 GHz, consistent with the radio observations of the GRB 970508's afterglow (Frail 1997). Note that an electron parameter ε_{el} below equipartition leads to higher optical depths at 4.9 GHz and that ν_{ab} depends weaker on the other model parameters.

If there is a flat, low energy tail of electrons factor below γ_m, so that $dN_e/d\gamma_e \propto \gamma_e^0$ as considered by Vietri (1997) and Waxman (1997a), then the self-absorption frequency is $\nu_{ab} = 2.8\, \varepsilon_{mag}^{-1/4} \varepsilon_{el}^{-1} n_0^{1/4} [(z+1)/2]^{-1} T_d^0$ GHz if electrons are radiative, and $\nu_{ab} = 9.3\ \varepsilon_{mag}^{1/4} \varepsilon_{el}^{-1/2} n_0^{1/2} E_{52}^{1/4} [(z+1)/2]^{-3/4} T_d^{-1/4}$ GHz for adiabatic electrons. With the usual parameters, $\nu_{ab} = 11\, T_d^0$ GHz for radiative electrons and $\nu_{ab} = 12\, T_d^{-1/4}$ GHz for adiabatic electrons, implying optical thickness at 4.86 GHz for $T < 37$ days. However, the remnant optical thickness at this frequency can be substantially lower if the ejecta was initially beamed and if, at low bulk Lorentz factors, the shocked fluid expands outside the cone, leading to a stronger deceleration than predicted by equation (6). If the effect of this sideways escape of the fluid is parameterized by including an extra factor $-A$ (with $A > 0$) in the exponent of T in equation (6), then $\nu_{ab} = 12\, T_d^{-(A+1/4)}$ GHz for adiabatic electrons, yielding optical thinness at 4.86 GHz at times $T > 5$ days if $A > 1/3$. Such a power-law approximation is suitable only for short times, as the decay of Γ due to the sideways escape is in fact exponential (Rhoads 1997): $\Gamma \propto \exp(-t/t_{se})$, where $t_{se} = (2\,\kappa \Gamma_0^2 \theta_{jet}^2)^{1/3}\, t_{dec} = 2.5\, (\Gamma_0/500)^{2/3} (\theta_{jet}/1^{\rm o})^{2/3} (\kappa/0.1)^{1/3}\, t_{dec}$, κ being the fraction of the initial energy contained in the remnant at the onset of the adiabatic phase (assumed to start before the effect of the sideways expansion becomes important) and θ_{jet} being the half-angular opening of the jet.

Throughout this work it was assumed that the external medium is homogeneous. For a medium varying as a power law in the distance and considering only the case of a relativistic remnant and a power-law spectrum $F_\nu = (\nu/\nu_p)^a F_{\nu_p}$, one finds that $F_\nu \propto T^{[4-\alpha+a(24-7\alpha)]/(14-4\alpha)}$ for a radiative remnant, $F_\nu \propto T^{(3a+1)/2}$ for radiative electrons in an adiabatic remnant and $F_\nu \propto T^{(3a/2)-[\alpha/(8-2\alpha)]}$ for adiabatic electrons, where $\alpha < 3$ is the index of the external fluid density: $n_{ext} \propto r^{-\alpha}$. If the external medium index changes from $\alpha = 0$ (homogeneous medium) to $\alpha = 2$ (pre-ejected wind), then the exponent of T in the previous expressions for the evolution of F_ν changes from $(2/7)(6a+1)$ to $(1/3)(5a+1)$ for a radiative remnant, is constant for an adiabatic remnant with radiative electrons, and varies from $3a/2$ to $(3a-1)/2$ for an adiabatic remnant. Therefore, the slope of the decay of F_ν is altered significantly by the external medium density index only if the electrons are adiabatic. The size of the adiabatic remnant evolves as $R_\perp \propto T^{(5-\alpha)/(8-2\alpha)}$, which gives $R_\perp \propto T^{5/8}$ for $\alpha = 0$ and $R_\perp \propto T^{3/4}$ for $\alpha = 2$. Thus, at given observer time, the remnant interacting with a pre-ejected wind appears larger than one running into a homogeneous external medium. When electrons are adiabatic, the self-absorption frequency evolves as $\nu_{ab} \propto T^{-3\alpha/(20-5\alpha)}$, which shows that, while ν_{ab} is constant in time for a homogeneous external medium, it decreases in time as $T^{-3/5}$ for a pre-ejected wind. It can be shown that electrons become adiabatic earlier in a pre-ejected wind and that the time when the remnant becomes non-relativistic increases strongly with the external medium density index, the evolution remaining relativistic up to tens of years in the pre-ejected wind case.

In the analytic derivations above we made several assumptions regarding the isotropy of the ejecta, the electron radiative regimes and the viewing geometry, which could lead to substantial inaccuracies in the analytical power-laws describing the evolution of F_ν, that are used in comparisons between observations and predictions of the fireball model: (1) the ejecta are isotropic (see Mészáros et al. 1998 for the wide variety of slopes that can be obtained in non-isotropic models); (2) all electrons are assumed in the same radiative regime as those with the minimum Lorentz factor (which leads to shallower spectral slopes at high frequency), although the times when electrons with different γ_e become adiabatic may span more than two orders of magnitude; (3) at fixed time, the observer receives radiation emitted at a unique lab-frame time (photons arriving simultaneously at detector may have been emitted by gas shocked at different Lorentz factors; such mixing of radiation leading to a weaker spectral evolution of the afterglow); (4) the reverse shock emission can be neglected (low frequency radiation received from this shock leads to shallower spectra in the infrared and to a continuous decay of the radio fluxes, hindering the rise of the forward shock emission in the early afterglow); (5) the model parameters for minimum electron Lorentz factor and magnetic field strength are constant in time (parameters decaying as a power-law yield steeper rises of the low energy light-curves and steeper decays of the fluxes at high frequency). Approximations (1) and (5) are also made in the numerical calculations. Further complications may arise if the ejecta is beamed in a jet (Rhoads 1997) or if the external medium is inhomogeneous.

4. Discussion

Summarizing, the features of the bursts and afterglows arising from impulsive or wind fireballs with a strong or weak coupling of electrons with baryons and magnetic field, are:

1. Wind fireballs produce softer GRBs than impulsive ones for the same set of hydrodynamical and energy release parameters, and increase the efficiency of the reverse shock, yielding a brighter optical and UV counterpart. An appropriate change in model parameters (particularly Γ_0) could shift the softer spectrum produced by wind fireballs into the γ-ray domain, but the fact that the GRB efficiency is lower

than in the impulsive model makes this possibility less likely to be a real scenario.

2. Strong coupling in the post-shock fluid leads to harder spectra and to a radiative phase of the afterglow which extends to later times than in the weak coupling case. It could explain the X-ray paucity observed in many GRBs, by maintaining for longer times higher electron Lorentz factor and, implicitly, the synchrotron emission from the blast wave in the γ-ray range.

3. At the same observer time, the intensity of the emission of a strong coupling remnant at lower energies (radio) is considerably weaker than that of a weak coupling one. In our simulations, an isotropic fireball with strong coupling requires 10^{53} ergs to yield radio fluxes comparable to those observed in the afterglow of GRB 970508, which is one order of magnitude larger than that necessary for a weak coupling fireball.

4. Unless the initial fireball Lorentz factor is substantially higher than considered here, the parameters describing the magnetic field strength and the electron energy must not be too much below equipartition, otherwise the main burst would have a spectral peak below ~ 50 keV. As a consequence of this, the remnant is not adiabatic in the early afterglow. The adiabatic phase starts earlier for a weak coupling remnant than for one with strong coupling.

5. During the afterglow, the flow Lorentz factor of the shocked fluid has only a weak dependence on the initial burst parameters, including the fireball initial Lorentz factor, so that GRBs with very different peak fluxes and γ-ray durations, arising from fireballs interacting with homogeneous surrounding media, should be followed by afterglows whose time-scales are similar.

The results of the numerical hydrodynamic calculations presented here are meant to be illustrative, and are not intended as fits, but rather as a study of the observable consequences of various physical assumptions about the energetic and dynamics which are possible in realistic models. An exploration of the parameter space will be needed, as well as consideration of some effects not included in the simplified model used here, such as anisotropic distribution of energy in the ejecta, inhomogeneous external medium, time-varying energy release parameters, or jet-like ejecta, in order to provide a more detailed characterization of the external shock model and comparison with the observational material on bursts and their afterglows.

This research has been supported by NASA NAG5-2857 and NAG5-2362.

REFERENCES

Blandford, R. D. & McKee, C. F. 1976, Phys. Fluids, 19, 1130

Crider, A. et al. 1997, ApJ, 479, L39

Frail, D. 1997, Nature, 389, 261

Meegan, C., Preece, R. & Koshut, T. 1998, *Gamma-Ray Bursts, Fourth Huntsville Symposium* (New York:AIP), in press

Mészáros , P. & Rees, M. J. 1993, ApJ, 405, 278

Mészáros , P. & Rees, M. J. 1997, ApJ, 476, 232

Mészáros , P., Rees, M. J., & Wijers, R. 1998, ApJ, accepted (astro-ph/9709273)

Mitrofanov, I. G. et al. 1996, ApJ, 459, 570

Panaitescu, A. & Mészáros , P. 1998a, ApJ, 492, 683

Panaitescu, A. & Mészáros , P. 1998b, ApJ, 493, L31

Preece, R. D. et al. 1998, in *Gamma-Ray Bursts, Fourth Huntsville Symposium*

Reichart, D. 1997, ApJ, 485, L57

Rhoads, J. E. 1997, ApJ, 487, L1

Rees, M. J. & Mészáros , P. 1992, MNRAS, 258, 41p

Rees, M. J. & Mészáros , P. 1994, ApJ, 430, L93

Sari, R. & Piran, T. 1997, ApJ, 485, 270

Strohmayer, T. E., Fenimore, E. E., Murakami, T., & Yoshida, Y. 1998, ApJ, accepted (astro-ph/9712332)

Tavani, M. 1997, ApJ, 483, L87

Vietri, M. 1997, ApJ, 488, L105

Waxman, E. 1997a, ApJ, 489, L33

Waxman, E. 1997b, ApJ, 491, L19

Wijers, R., Rees, M. J., & Mészáros , P. 1997, MNRAS, 288, L51

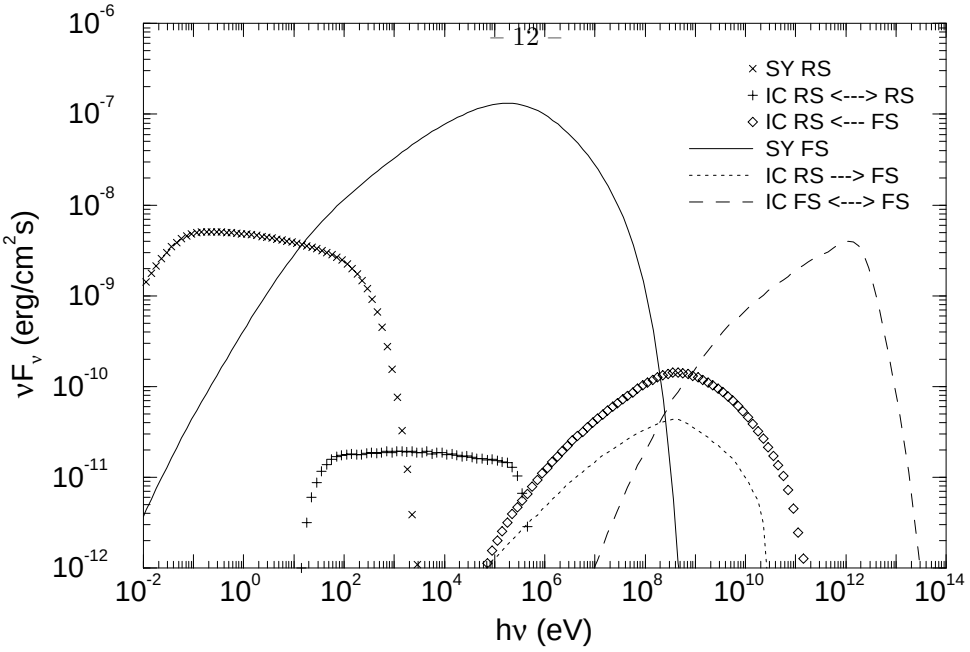

Fig. 1.— Spectrum of a GRB arising from an impulsive fireball and with a weak coupling in the radiating ejecta. The burst was obtained assuming an initial energy release of 10^{52} ergs/sr, and a fireball with initial Lorentz factor $\Gamma_0 = 500$; the magnetic field, protons and electrons are at equipartition; the electron distribution power-law index is $p = 2.5$ and γ_M/γ_m is 100 for the reverse shock and 10 for the forward shock. The burst is located at a redshift $z = 1$. The legend indicates the origin of each component, e.g. RS → FS means reverse shock synchrotron photons up-scattered behind the forward shock.

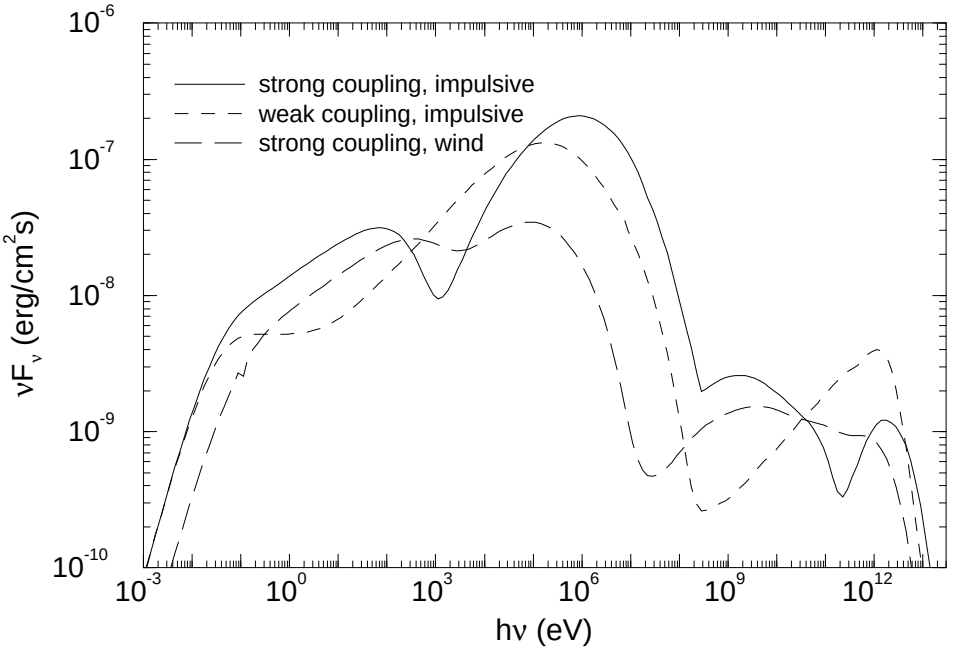

Fig. 2.— Comparison between averaged spectra obtained in three models (see legend). The burst parameters are the same as for Figure 1. Note the harder and more intense burst resulting from an impulsive fireball and strong coupling, as well as the weaker self-inverse Compton emission from the forward shock (around 1 TeV). An extended energy release at the place where the fireball originates results in a softer burst, in which the two shocks radiate comparable amounts of energy.

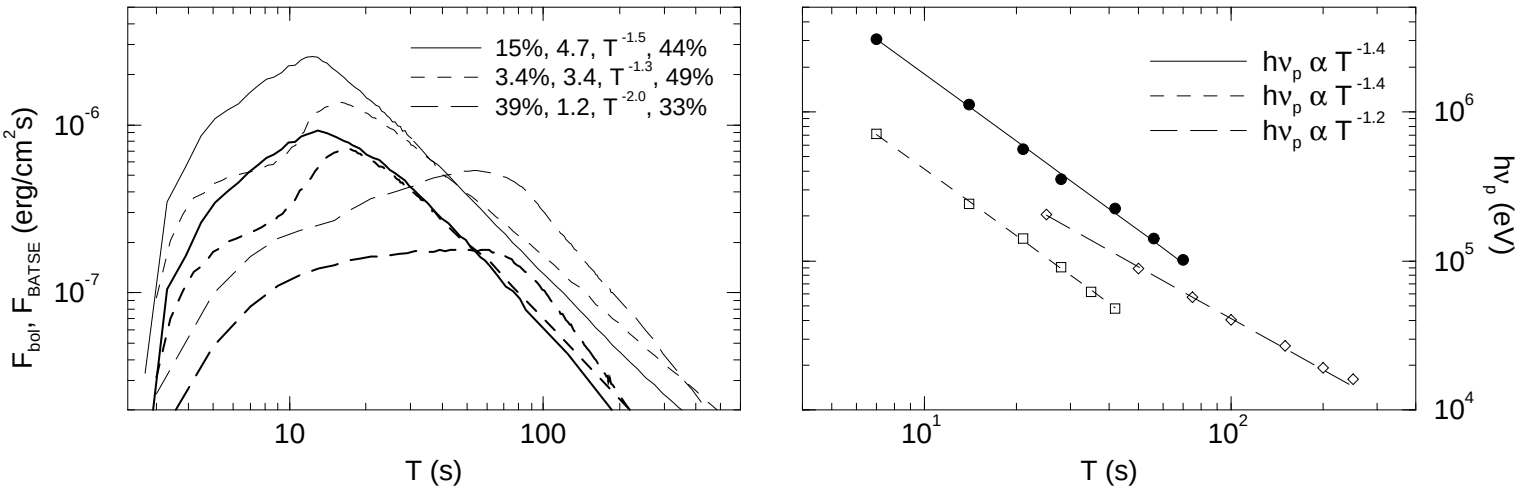

Fig. 3.— Temporal and spectral evolution of the bursts whose spectra are shown in Figure 2. The left graph shows in log-log scale the observed bolometric flux (thin curves) and the flux in the 25 keV – 1 MeV range (thick curves). The legend gives for each model the fractional fluence of the reverse shock, the light-curve temporal asymmetry, the burst $T^{-\alpha}$ fall and its efficiency (see text for definitions). The right graph shows the evolution of the peak of νF_ν. The types of lines used are the same as in Figure 2: solid for impulsive and strong coupling, short dashes for impulsive and weak coupling, and long dashes for wind and strong coupling.

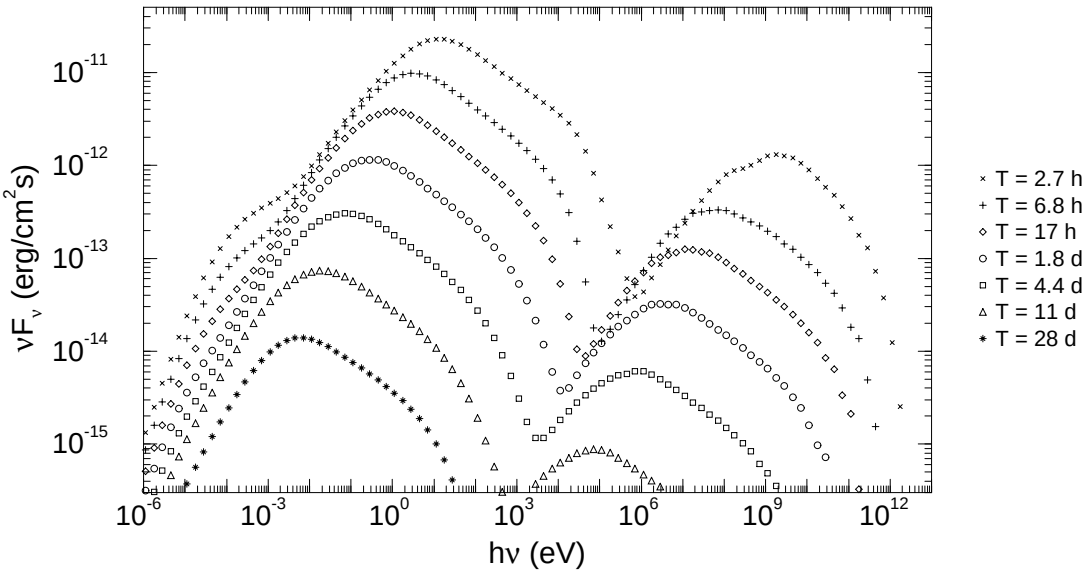

Fig. 4.— Left graph: spectral evolution of the afterglow in the weak coupling model (this is the afterglow of the GRB shown in Figure 1, but using $\gamma_M/\gamma_m = 100$). The legend indicates the observer time for each spectrum.

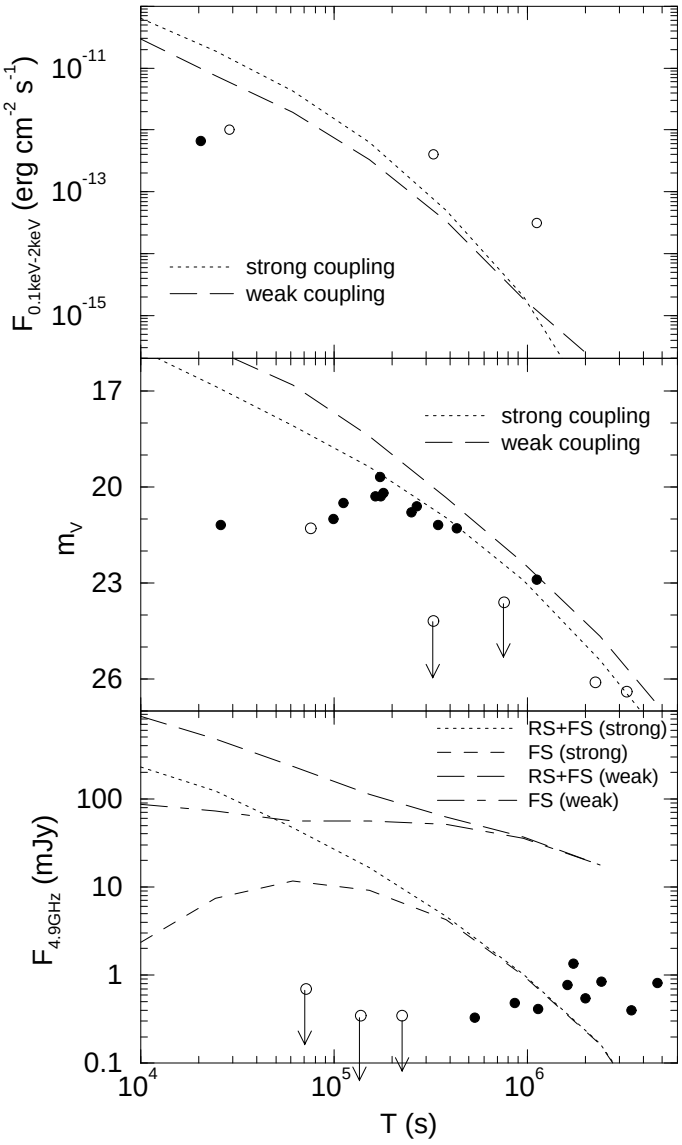

Fig. 5.— Fluence of numerically simulated afterglows in the 0.1 keV − 2 keV band, their V magnitudes and flux densities in radio (4.9 GHz), for both strong and weak coupling models. Symbols denote real bursts: GRB 970228 (open circles) and GRB 970508 (filled circles), arrow showing upper limits. When relevant, the fluxes from the forward shock and from both shocks have been shown separately (see legends of lower graphs).